CHAPTER 116

LONG-PERIOD OSCILLATIONS IN A HARBOUR CAUSED BY TYPHOON

Wataru Kioka[1]

ABSTRACT

A nonlinear model for predicting the resonant oscillations in a harbour due to typhoon is developed and its validity is evaluated through the comparisons with filed measurements obtained in Yui Fishery Harbour facing Suruga Bay in Japan. The numerical model is based on a time domain solution of Boussinesq equations proposed by Nwogu(1993) with an additional Forchheimer resistance term in the momentum equation to take account of the reflection characteristics of permeable seawalls in the field. It is shown that the numerical model predicts well the low-frequency oscillations inside the harbour exited by incident wave groups.

1. INTRODUCTION

Excessive long-period oscillations are often observed in relatively small harbours along sea coasts when typhoons or atmospheric low pressures pass over sea area. Such oscillations often lead to the breaking of mooring lines and the flooding on the wharf. Recent filed observations reveal that locked or bound long waves accompanied by incident wave groups have relevance to large oscillations in a harbour (e.g., Okihiro *et al.*, 1993). The resonance phenomena due to such infragravity forcing are essentially nonlinear as the locked long waves exist under wave groups through nonlinearity. In this study, a nonlinear model for predicting the low-frequency oscillations inside a harbour due to the typhoon is developed using the Boussinesq equations. The validity of the model is evaluated through the comparisons with field measurements obtained during Typhoon in Yui Fishery Harbour facing Suruga Bay in Japan.

2. MATHEMATICAL MODEL

[1] Professor, Dept. of Civil Eng., Nagoya Institute of Technology, Nagoya, 466 Japan.

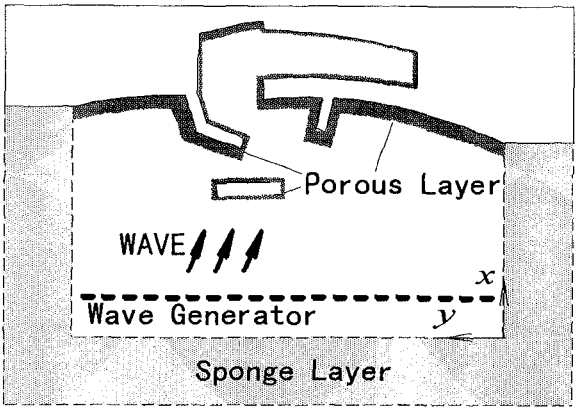

Fig. 1 Sketch of numerical model

2.1 Model Equations

The numerical model is based on a time domain solution of Boussinesq equations proposed by Nwogu (1993) with an additional absorbing term in the momentum equation and a source generation term in the continuity equation (Brorsen and Larsen, 1987) :

$$\zeta_t + \nabla\cdot\left[(\zeta+h)\boldsymbol{u}\right] + \nabla\cdot\left[\left(\frac{1}{2}z_\alpha^{\,2}-\frac{1}{6}h^2\right)h\nabla(\nabla\cdot\boldsymbol{u}) + \left(z_\alpha+\frac{1}{2}h\right)h\nabla\{\nabla\cdot(h\boldsymbol{u})\}\right] - U^* = 0 \qquad (1)$$

$$\boldsymbol{u}_t + (\boldsymbol{u}\cdot\nabla)\boldsymbol{u} + g\nabla\zeta + \left[\frac{1}{2}z_\alpha^{\,2}\nabla(\nabla\cdot\boldsymbol{u}_t) + z_\alpha\nabla\{\nabla\cdot(h\boldsymbol{u}_t)\}\right] + f_s\left[\boldsymbol{u} + \left[\frac{1}{2}z_\alpha^{\,2}\nabla\cdot(\nabla\cdot\boldsymbol{u}) + z_\alpha\nabla\{\nabla\cdot(h\boldsymbol{u})\}\right]\right] = \boldsymbol{0} \qquad (2)$$

where $\zeta(x,y)$ is the water surface elevation, $\boldsymbol{u}(x,y,t)$ is the velocity at an arbitrary elevation $z=z_\alpha(x,y)$, U^* is the vertical source distribution extending from the bottom to free surface, and $f_s(x,y)$ is the distribution function for the sponge layer. The instantaneous horizontal volume flux of the source distribution is included only in the continuity equation, provided that the weak nonlinearity represented by the ratio of wave amplitude to water depth, $\varepsilon = a_0/h_0$, is in the same order of magnitude as the frequency dispersion represented by the square of the ratio of the water depth to wavelength, $\mu^2 = (h_0/l_0)^2$. The distance z_α is determined using an error-minimizing criterion for the dispersion relation. Following Nwogu (1993), the elevation z_α is set

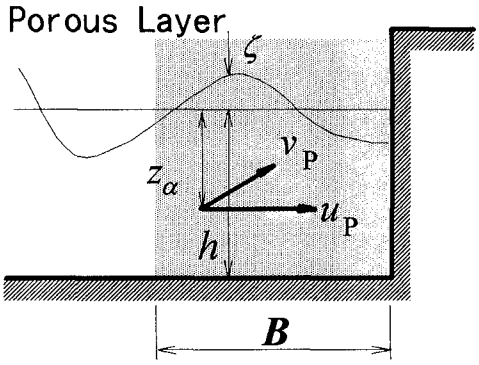

Fig. 2 Definition sketch of porous structure model

to be $-0.53h$. On the upwave control boundary and sides of the computational domain, all outgoing waves are absorbed by using sponge layers and applying the Sommerfeld radiation condition at the outer boundaries of the sponge region (see Fig. 1). The radiation condition is prescribed from the linear long wave theory. The function $f_S(x,y)$ varies linearly over the sponge region, i.e. increases linearly with the distance from fluid boundary lines, so that local disturbances due to the sponge layers are kept to a minimum. A harbour with fully reflective boundaries is treated as the solid walls.

2.2 Modeling Porous Structures

For the cases of partially reflective boundaries, the Boussinesq equations (1) and (2) are further modified to account for the reflection characteristics of permeable seawalls, assuming Forchheimer resistance law for the fluid motion in porous structures, as in the forms (Kioka et al., 1996)

$$\zeta_t + \nabla\cdot[(\zeta+h)\boldsymbol{u}_P] + \nabla\cdot\left[\left(\frac{1}{2}z_\alpha{}^2 - \frac{1}{6}h^2\right)h\nabla(\nabla\cdot\boldsymbol{u}_P) + \left(z_\alpha + \frac{1}{2}h\right)h\nabla\{\nabla\cdot(h\boldsymbol{u}_P)\}\right] = 0 \tag{3}$$

$$\frac{\tau}{\lambda}\boldsymbol{u}_{Pt} + \frac{1}{\lambda^2}\frac{1}{2}\nabla\left(\boldsymbol{u}_P{}^2\right) + g\nabla\zeta + \frac{\tau}{\lambda}\left[\frac{1}{2}z_\alpha{}^2\nabla(\nabla\cdot\boldsymbol{u}_{Pt}) + z_\alpha\nabla\{\nabla\cdot(h\boldsymbol{u}_{Pt})\}\right] + \alpha\left[\boldsymbol{u}_P + \left[\frac{1}{2}z_\alpha{}^2\nabla(\nabla\cdot\boldsymbol{u}_P) + z_\alpha\nabla\{\nabla\cdot(h\boldsymbol{u}_P)\}\right]\right] + \beta|\boldsymbol{u}_P|\boldsymbol{u}_P = \boldsymbol{0} \tag{4}$$

where $\boldsymbol{u}_P$ is the discharge velocity vector at the distance z_α in porous structures, λ is the porosity, τ is the inertial coefficient given as $\tau = 1+\kappa(1-\lambda)$ with κ being the added mass coefficient, α and β are the linear and nonlinear damping coefficients in the unsteady Forchheimer equation, respectively. The flow in the porous domain is

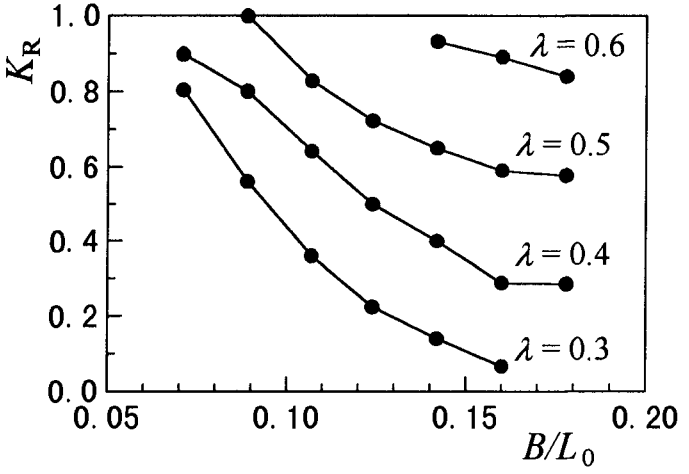

Fig. 3 Reflection coefficients ($h = 4.0$ m)

assumed irrotational. The damping coefficients α and β are respectively given after van Gent (1995) as

$$\alpha = 1000\frac{(1-\lambda)^2}{\lambda^3}\frac{\nu}{D^2} \tag{5}$$

$$\beta = 1.1\left(1+\frac{7.5}{KC}\right)\frac{(1-\lambda)}{\lambda^3}\frac{1}{D} \tag{6}$$

where ν is the kinematic viscosity coefficient, D is the mean grain size of the material of the porous media, and KC is the Keulegan-Carpenter number. The contribution of the added mass to the total inertial resistance is assumed to be disregarded ($\tau = 1$).

The damping coefficients of porous structures cannot be exactly determined from the field measurements, as methods for evaluating these coefficients of large blocks are, at present, not fully established. In the numerical analysis, the porosity λ is adjusted to suit the observed reflection coefficients while the damping coefficients α, β are held fixed. Fig. 3 shows the computed reflection coefficients K_R as a function of the ratio of the thickness of porous body B to the deepwater wavelength L_0, using sinusoidal waves in the constant water depth of $h = 4.0$ m. The coefficients K_R are simply given as the ratio of the maximum wave height measured in front of the porous structure to the incident wave height. For example, in the case of wave period $T = 9.5$ s and $B = 20$ m, the porosity $\lambda = 0.4$ approximately gives $K_R = 0.4$, according to Fig. 3. The energy dissipation of the incident waves due to the porous

the porous structure, however, decreases with the increase of the water depth. In the case of $h = 6.0$ m, K_R nearly equals 1.0 in the range of $\lambda > 0.4$ and $B/L_0 < 0.2$. For porous structures in relatively deep water depths, the reflection coefficients are underestimated even when using an unrealistic value of the porosity λ. In the deeper water depth, the thickness of the porous structure B is then taken longer than the actual width of the wave-dissipating blocks in the field. The wider porous body leads to better agreements with the observed reflection coefficients, but yields slightly different reflection characteristics of the short waves.

2.3 Numerical Scheme

The equations (1)-(4) are numerically solved using a finite difference scheme. The spatial derivatives in one direction are approximated using 5grid-point centered differences with fourth-order accuracy, leading to a truncation error that is small relative to all retained terms in the equations. Although the finite difference approximations of the xy-, xxy- and yyx-derivatives can be respectively approximated with fourth-order accuracy using 3grid-point centered differences per a direction, 5grid-point approximations are adopted here in order to avoid numerical instabilities. For the temporal integral, an iterative scheme based on the 3rd-order Adams-Bashforth-Moulton method is employed. The water surface elevation ζ can be obtained explicitly. As the velocity component in the x-direction u is solved by calculating matrices, the derivatives of the component in the y-direction v can be treated explicitly for the sake of efficient calculations.

The directional spreading of incident wave energy has a significant influence on the long-period oscillations, and thus must be taken into account for the quantitative prediction. The wave condition at the upwave boundary is then specified in terms of a directional wave spectrum. The single direction per frequency method is used to describe the first-order water surface elevations with the parametric cosine power function for the directional distribution. Since the contribution of second-order waves, especially sub-harmonic waves, is important for the quantitative prediction, i.e., for preventing the generation of spurious free waves at the incident boundary, all the sub-harmonics and super-harmonics in directional wave fields are included in the incident waves through the quadratic transfer function. The characteristics of the groupiness of individual waves and the associated long-period waves are influenced by the initial phase angles of the different frequency components. In the numerical analysis hereafter, the computations are carried out three times for each set of the initial phases. The effective duration of each run is about 1200s.

3. FIELD OBSERVATIONS

Yui Fishery Harbour is a relatively small harbour facing Suruga Bay in Japan (see Fig. 4). Two breakwaters are constructed at the eastern and western side of the harbour entrance, and the offshore breakwater (under construction) is located about 70 m away from the tip of the western breakwater. These breakwaters and the

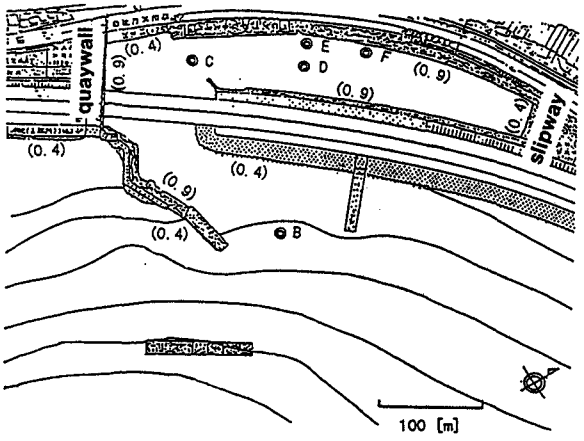

Fig. 4 Layout of Yui Fishery Harbour

revetments facing open sea are covered with wave dissipating blocks. The field measurements of the water surface elevations have been carried out for two months from August to October in 1994, at station about 300 m offshore from the southern offshore breakwater, station at the harbour entrance and 4 stations inside the harbour basin, as shown in Fig. 4. The time series of surface elevation with the significant wave height $H_{1/3} = 3.7$ m and period $T_{1/3} = 9.5$ s have been obtained at the offshore station due to Typhoon 26, September 29-30 in 1994. The wave heights of the short-wave components were significantly reduced inside the harbour. The low-frequency waves in the range from 0.0025 Hz to 0.013 Hz were, however, amplified to a certain degree due to resonant oscillations inside the harbour.

4. NUMERICAL CONDITIONS AND RESULTS

4.1 Numerical Conditions

The directional spectra have not been observed at the offshore station. The measured time series of the surface displacements cannot be directly used for the incident waves in the numerical calculations. The incident short-wave components are given from the Bretschneider-Mitsuyasu spectrum assuming the Mitsuyasu-type directional function for the directional distributions. The water depth at the offshore station is 25.0 m. The significant wave height $H_{1/3} = 3.7$ m and the period $T_{1/3} = 9.5$ s observed during Typhoon 26, 1994 are used for the numerical simulations. The parameter S_{max} indicating the degree of directional spreading was not directly measured but estimated from the measured wave steepness using the procedure proposed by Goda and Suzuki (1975). Their estimation method gives $S_{max} = 40$ at

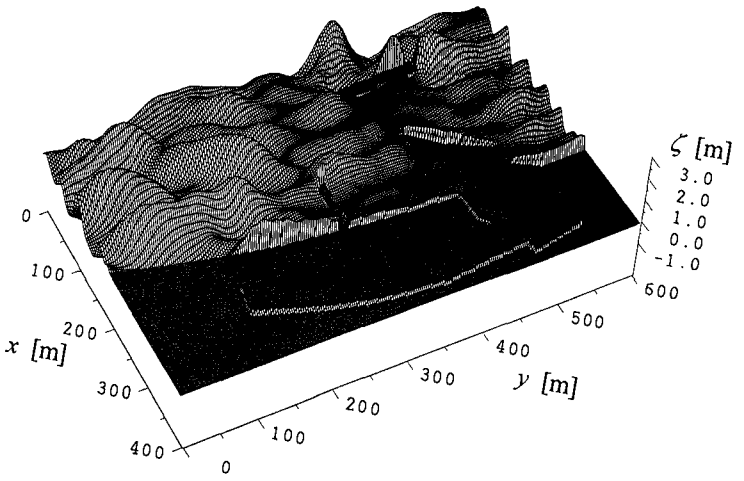

Fig. 5 Snapshot of free-surface displacements

the offshore station. The frequency bands of $0.4 \sim 2.0$ times the peak frequency are decomposed into 100 first-order wave components. The directional spread of $\pm 50°$ from the principal wave direction is modeled using 20 components. The wave directions are selected in a random order within each frequency band. The set-down wave components defined as low-frequency waves below the bands of short-waves are calculated through the quadratic transfer function, and are added to the short-waves at the incident boundary. The super-harmonic wave components are also included, but with no effect on the long-period oscillations in the harbour. Since the inclusion of all second-order waves requires a large computational effort, only the contribution of the sub-harmonic components may be considered for the second - order waves. The numerical simulation is carried out using a time interval $\Delta t = 0.1$ s, and spatial grid sizes $\Delta x = 5$ m, $\Delta y = 5$ m.

The water depths at each grid-points are counted, referring to the mean water level observed at the offshore station. The 1: 6 constant slope slipway is located at the end of harbour basin. The short-wave components are expected to break on the slope. The wave heights are, however, very small inside the basin, so that the influence of long-period free waves caused by the wave breaking on the slope of the slipway may be disregarded for predicting the harbour oscillations. The slipway inside the harbour is then assumed to be an upright porous structure similar to the other partially reflective boundaries.

4.2 Numerical results

Fig. 5 shows the snapshot of the free-surface displacements in the vicinity of Yui Fishery Harbour due to Typhoon 26, 1994. The offshore breakwater, being under

construction, is not effective in reducing the transmitted waves on the leeward side. The incoming short-waves considerably attenuate inside the harbour basin primarily by the breakwaters and the wave absorbing works.

The comparisons of the time series between the numerical results and the observations are shown in Fig. 6. In the case of offshore station, the temporal profiles of the long-period components are exaggerated by multiplying by 5. The set-down waves generated by the short-waves crossing at small angle tend to be underestimated in the region of relatively deep water depth. This may result in the slightly smaller long-period components as compared with the observations at the offshore station. At the station D inside the basin the low-frequency oscillations near 0.013 Hz are clearly reproduced, but their amplitudes are slightly smaller than the measured ones. The computed short-wave components inside the basin appear to be calmer than the measurements. The wave dissipation inside the harbour is possibly overestimated from the porous structure model.

The computed spectra at the stations C and D inside the harbour are compared with the measurements in Fig. 7. The numerical model predicts well the amplification in the low-frequency range. It should be noted the secondary peak near 0.013 Hz is slightly larger than the first peak near 0.0025 Hz. The linear model gives much smaller amplification for the secondary peak.

The spatial profiles of the long-period components are plotted in Fig. 8. The long-period components of near the peak frequencies $f = 0.0025$ Hz, 0.0090 Hz and 0.013 Hz are extracted from the computed spectra inside the harbour. The long-period oscillations are seen to be not multi-directional, but quite uni-directional in the y-direction (in the direction of the longer side of the basin). Near the first peak ($f = 0.0025$ Hz), the surface elevations within the harbour rise more or less in unison. At the second and third peaks (0.0090 Hz, 0.013 Hz), the long-period waves behave as a standing wave, respectively corresponding to two and three anti-nodes in the y-direction.

5. CONCLUDING REMARKS

A nonlinear model, which takes account of the multi-directional features of the incoming waves as well as the partially reflecting boundaries, is developed for predicting the resonant oscillations in a harbour due to typhoon. The spectra observed in Yui Fishery Harbour are well reproduced in the low-frequency range of interest by the present numerical model. Possible countermeasures against the resonant oscillations observed in a small harbour like Yui Fishery Harbour are currently under investigation using the present model.

ACKNOWLEDGEMENTS

The research has been funded by the Grand-in-Aid for Scientific Research from the Ministry of Education, Science and Culture of Japan. The author would like to thank Dr. M. Tanaka of Shimz Corp. and Yui Fisheries Co-operative Organization for

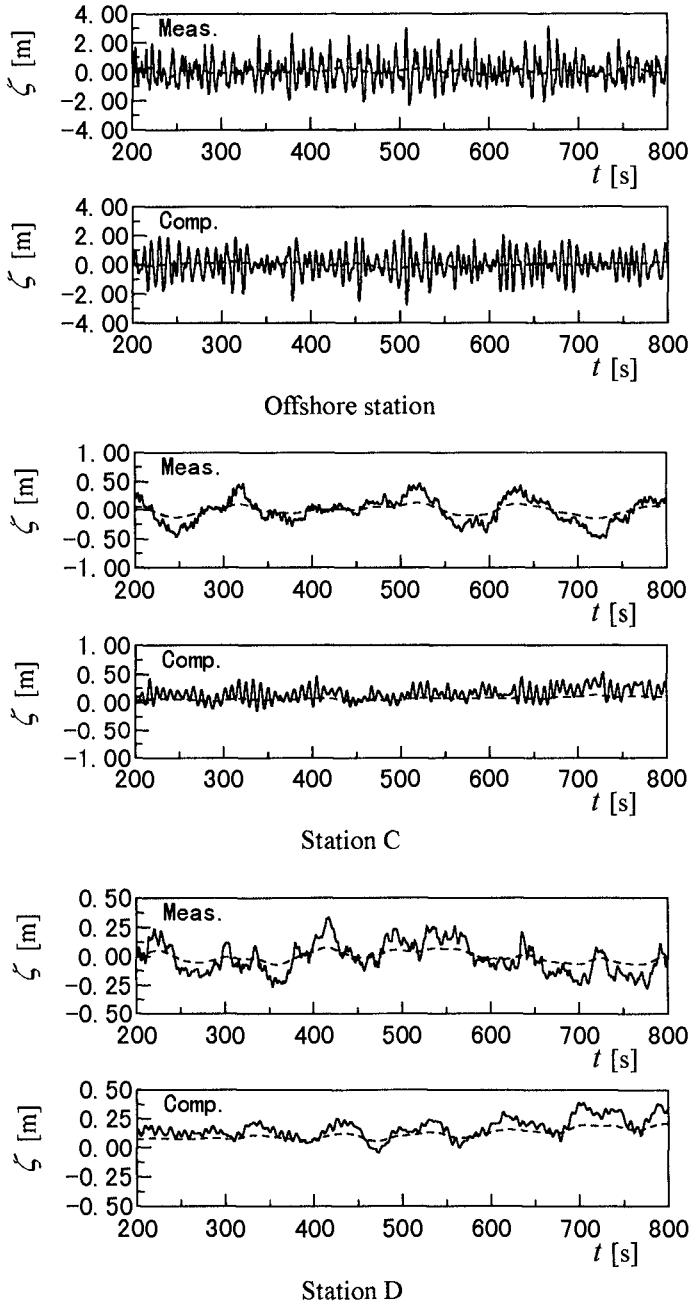

Fig. 6 Comparison of temporal profiles (- - - - - : long-wave components)

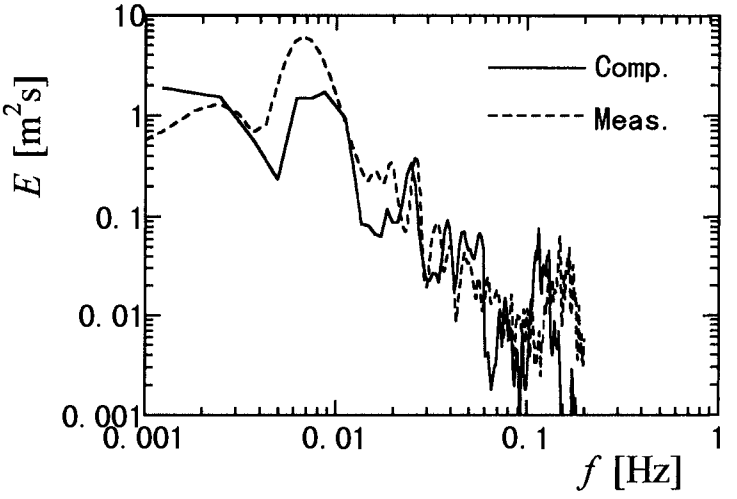

Station C

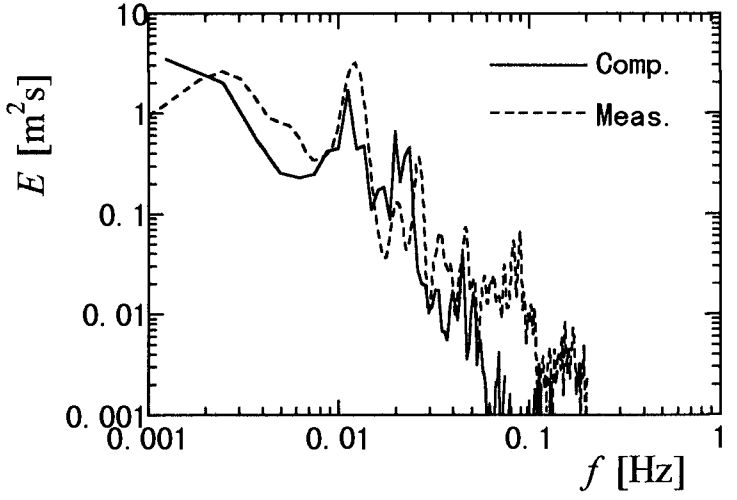

Station D

Fig. 7 Comparison of spectra inside the harbour

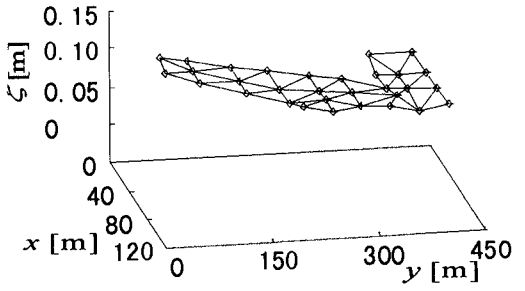

(a) f = 0.0025 Hz

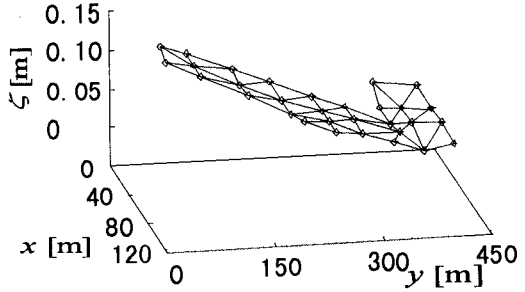

(b) f = 0.0090 Hz

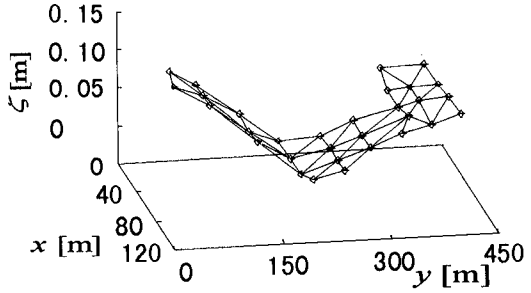

(c) f = 0.0130 Hz

Fig. 8 Spatial profiles of long-period wave components

their contribution and cooperation in obtaining the filed data. Thanks are also due to K. Kashihara and H. Aikawa for their assistance in carrying out the numerical simulations.

REFERENCES

Brorsen, M. and Larsen, J. (1987) : Source generation of nonlinear gravity waves with the boundary integral equation method, Coastal Eng., No. 11, pp. 93-113.

Goda, Y. and Suzuki, Y. (1975) : Computation of refraction and diffraction of sea waves with Mitsuyasu's directional spectrum, Technical Note of the Port and Harbour Research Institute Ministry of Transport, No. 230, pp.4-18 (in Japanese).

Kioka, W., Kai, H. and Yasue, T. (1996) : Numerical analysis of wave deformation over a porous bottom by Boussinesq equations, Proc. Coastal Eng., JSCE, Vol.43, pp.101-105 (in Japanese).

Nwogu, O. (1993) : Alternative form of Boussinesq equations for nearshore wave propagation, J. Waterway, Port, Coastal, and Ocean Eng., Vol. 119, No.6, pp. 618-638.

Okihiro, M., Guza, R. T. and Seymour, R. J. (1993) : Excitation of seiche observed in a small harbor, J. Geophys, Res., Vol. 98, pp. 18201-18211.

van Gent, M. R. A. (1995) : Porous flow through rubble-mound material, J. Waterway, Port, Coastal and Ocean Eng., Vol. 121, No. 3, pp.176-181.